# Confocal polarization imaging in high-numerical-aperture space

**C. Macias-Romero,[1] M. R. Foreman,[2] P. R. T. Munro,[3] and P. Török[4,*]**

[1]*Laboratory of Fundamental Biophotonics, École Polytechnique Fédérale de Lausanne, Lausanne, Switzerland*

[2]*Max Planck Institute for the Science of Light, Laboratory of Nanophotonics and Biosensing, 91058 Erlangen, Germany*

[3]*Optical+Biomedical Engineering Laboratory, School of Electrical, Electronic & Computer Engineering, The University of Western Australia, Crawley, WA 6009, Australia*

[4]*Blackett Laboratory, Imperial College London, London SW7 2BZ, UK*

**Corresponding author: peter.torok@imperial.ac.uk*

Received November 28, 2013; revised March 11, 2014; accepted March 11, 2014; posted March 13, 2014 (Doc. ID 202205); published April 8, 2014

In this work we describe theoretical and experimental physical aspects of high-resolution imaging polarimetry and its application to polarization-multiplexed encoding. We theoretically demonstrate that it is possible to resolve the orientation of two fixed dipole-like emitters placed significantly below the resolution limit if their emission is uncorrelated. Furthermore, we experimentally demonstrate this phenomenon by illuminating closely spaced asymmetric nanopits with unpolarized light and subsequently determining their individual orientation and position from the measured spatial distributions of the azimuth angle of the polarization and degree of polarization, respectively. Reduction of the optical resolution of the imaging system is also shown to only weakly affect resolution obtainable via polarization measurements. 

*OCIS codes:* (180.1790) Confocal microscopy; (110.5405) Polarimetric imaging; (210.0210) Optical data storage.
http://dx.doi.org/10.1364/OL.39.002322

Optical polarimetry, and polarization imaging, is the measurement and characterization of the spatial variations of the polarization state of light, which can additionally allow polarization properties of an object, such as birefringence, to be studied. While these techniques have been extensively employed on the millimeter and micrometer scales [1], particularly for objects exhibiting natural optical activity, e.g., dichroism or birefringence, their use to study nanometer scale variations has received little attention despite their potential [2,3]. In the context of microscopy, particularly in high numerical aperture (NA) systems, polarimetry is commonly considered a simple add-on measurement that may afford additional information, e.g., contrast enhancement. Accordingly, it is common belief that polarization imaging follows the same rules as conventional imaging, such that nanometer scale variations are not resolvable, as dictated, for example, by Abbe's resolution limit. We here, however, discuss a number of physical aspects of high-NA confocal polarization microscopy and demonstrate both theoretically and experimentally that this is not the case, mainly due to the great number of independent degrees of freedom afforded by complete polarimetry.

In the context of irradiance (intensity) imaging, the concept of resolution refers to the ability of an optical system to distinguish fine structures in the topography of an object from variations in the irradiance. Here, in the context of polarization imaging however, the concept of *resolution* must also take into account the variations in parameters describing the electric field of the light scattered by an object. Not only are the variations in the intensity considered in this concept, but also the spatial variations in the orientation (azimuth angle) of the polarization state, the degree of polarization (DOP), and the retardance between the components of the electric field. For example, consider imaging a few closely spaced molecules; these may appear unresolvable in the irradiance domain, while one could still resolve their orientation, if their positions are available, by measuring the spatial variations of the azimuth angle of the scattered electric field. Our interest in making this clarification is to lay the foundations for studying the loss of information that is present in any of these parameters upon propagation through an optical system. More specifically, here we show that the orientation of two dipoles placed significantly below Abbe's resolution limit can be resolved if they are illuminated with spatially uncorrelated light. We also study the scenario of $n$ dipoles evenly spaced below the diffraction limit and the effect of cross talk on the measured orientation; we show experimentally that their position can be obtained from the spatial distribution of the DOP and their orientation from the azimuth angle. These results are applicable, for example, to multiplexed data encoding, the characterization of plasmonic structures, and superresolution imaging techniques such as PALM or STED.

Discussion of resolution in scalar imaging systems traditionally follows by consideration of two point sources; however, in the paradigm of polarimetric imaging, dipole scatterers must instead be taken so as to account for polarization. We note that scattering from subwavelength structures is commonly well described by Rayleigh theory, such that the dipole model is appropriate. Consider then two fixed dipole scatterers illuminated by a tightly focused beam and imaged by a confocal setup [Fig. 1(a)]. When the illuminating focused beam is spatially uncorrelated, produced for example by unpolarized light [4], each dipole will emit a fully polarized field whose state of polarization is defined by its moment ($\mathbf{p}$) [5] and the amplitude is modulated according to the temporal variations of the incident polarization, i.e., $\mathbf{E}'(t) \propto \mathbf{p}|\mathbf{p}\cdot\mathbf{E}(t)|$. As the scattered fields propagate through the imaging system, the fields from each dipole

 

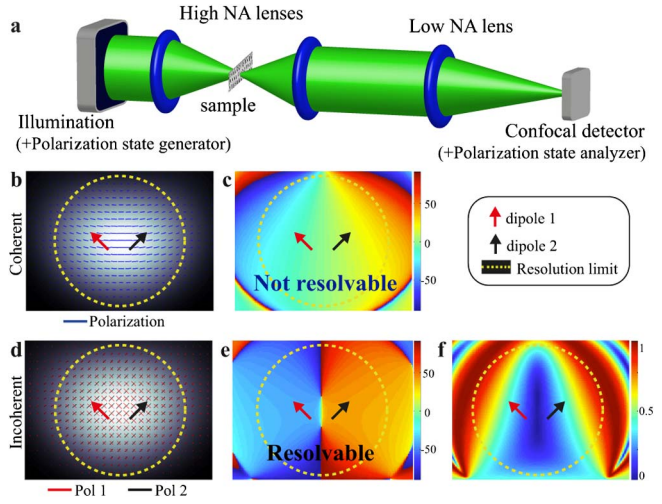


Fig. 1. Resolving the orientation of two dipole-like emitters placed below the diffraction limit. The imaging system is shown in (a) and polarization imaging simulations are shown in (b)–(f). Two fixed dipole-like emitters are placed below the resolution limit and illuminated with correlated (b), (c) and uncorrelated light (d)–(f). The dipoles are depicted by the black and the red arrows. The dotted circles depict the optical resolution of the system. The grayscale in (b) and (d) denotes irradiance, while the blue, black, and red line segments depict the polarization state of the field position-wise. (c) and (e) show the spatial distribution of the azimuth angle of the polarization given in (b) and (d), respectively. The spatial distribution of the DOP in (d) is shown in (f). It is possible to resolve the orientation of two fixed dipole-like emitters placed below the resolution limit in the case of uncorrelated illumination.

overlap spatially. If the amplitude modulations of the fields emitted by the dipoles are correlated (i.e., the focused beam possesses a high degree of spatial coherence), the polarization state of the fields combine coherently, yielding a smoothly varying polarization distribution in the image plane [Fig. 1(b)]. In this case, the orientation of the dipoles can be resolved only if the (irradiance) resolution of the imaging system allows it [Fig. 1(c)]. However, if the modulations are uncorrelated, the fields emitted by the dipoles combine incoherently [Fig. 1(d)], yielding a partially polarized field, which can be decomposed into fully polarized [Fig. 1(e)] and unpolarized components [Fig. 1(f)]. The polarized component is formed by the fully polarized fields emitted by the dipoles and, even if the dipole separation is smaller than the irradiance resolution limit, the orientation of the dipoles can be retrieved by isolating and scanning point-wise the polarized part of the field [Fig. 1(e)]. Note that the size of the confocal detector plays an important role due to the spatial averaging of the field occurring at this location [6,7]. We thus conclude that, by *temporal and spatial manipulation of the illuminating electric field, it is possible to resolve the orientation of two fixed dipole-like emitters placed below the resolution limit regardless of their separation*. This is a key finding of this Letter. Below, we present the scenario of $n$ evenly spaced dipoles and the experimental realization using a laser scanning confocal microscope capable of full polarization characterizations [8–10] [Fig. 1(a)].

While theoretically it is possible to resolve the orientation of the two dipoles independently of their separation when illuminated with uncorrelated light, the practical limit arises when the noise present in the system dominates over the DOP and from the possibilities of producing a spatially uncorrelated illumination [11]. In a more general case where multiple dipoles are considered, the ability of the system to resolve accurately their orientation depends on cross talk among all scatterers. For $n$ uncorrelated dipole sources evenly spaced in one dimension, the measured Stokes vector $\mathbf{S}(x)$ in the image plane can be simply expressed as the sum of the Stokes vectors $\mathbf{S}_i$ representing each dipole weighted by the point spread function of the system. Assuming a shift invariant imaging system we can thus write [12]

$$\mathbf{S}(x) = \sum_{i}^{n} \mathrm{PSF}(x - x_i) \cdot \mathbf{S}_i, \tag{1}$$

where $\mathrm{PSF}(x - x_i)$ is the point spread function of the imaging system centered around $x_i$, i.e., the Gaussian image point of the $i$th dipole. The PSF may be considered as either a scalar function or a point spread Mueller matrix [12] depending on the assumptions required in the treatment. A scalar PSF is, for example, more appropriate to low-NA imaging systems [13], while high-NA systems can significantly affect the polarization state of light, thus necessitating a matrix formalism [12]. The use of the Mueller–Stokes formalism to write Eq. (1) is justified because the dipole sources are assumed to be uncorrelated. In the case of a partial correlation, Eq. (1) would have to include a term that describes the combination of the coherent part of the fields.

When imaging fixed dipole sources, the azimuthal angle, $\theta$, of the polarization state in the image plane is determined by the dipole orientation. In the Stokes formalism $\theta = \tan^{-1}(s_2/s_1)/2$, where $s_j$ are the $j = 0\ldots3$ elements of the Stokes vector. When imaging multiple dipoles, the measured azimuthal angle [inferred from $\mathbf{S}(x)$] varies with position, as per Eq. (1). Note that the 2D Stokes formalism is valid only in the context of polarization imaging if a sufficiently small confocal detector or a low-NA lens is used to produce the image [6], so that the contribution of the longitudinal component of the field is negligible.

To illustrate the points above, we studied a set of nanostructures carved into a Si substrate by means of focused ion beam milling [shown in Fig. 2(a)]. Each nanostructure is a pit 50 nm wide, 200 nm long, and $\lambda/4 \approx$ 100 nm deep, and they are separated by 200 nm. Their angular orientations, which lie in the range of 45°–84°, were chosen to maximize intersymbol interference. The study was performed using the optical system depicted in Fig. 1(a) in a reflection configuration, using a 405 nm diode laser (Coherent Inc.) and an epiplan-apochromat DIC objective lens 0.95 NA (Zeiss).

When the sample is illuminated with unpolarized light, the scattered field becomes partially polarized (due to the polarizance that each individual pit exhibits), such that the polarized part of the field has a state of polarization that is aligned along the long axis of the nanostructures. Their angular orientations can thus be obtained by measuring the azimuth angle of the imaged field. Line

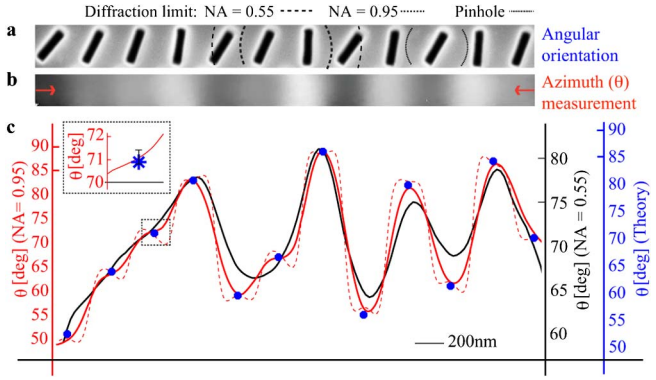


Fig. 2. Resolving the orientation of nanostructures with different numerical apertures. (a) Scanning electron microscope (SEM) image of a track of the nanostructures (200 nm× 50 nm × 100 nm, 200 nm apart) milled into an Si substrate. The dashed lines in a depict, as a reference, the sizes of the pinhole (scaled to high-NA space) and diffraction limits for 0.95 and 0.55 NA. The spatial distribution of the measured azimuth angle with 0.95 NA is shown in (b), from which a line scan is taken and shown in (c) (red, left axis = 0.95 NA; black, right axis = 0.55 NA). The dashed red line is from rigorous simulations of high-NA imaging systems. The blue markers depict the orientation of the nanostructures obtained from the SEM image. Accompanying error bars are shown magnified in the inset. Reducing the NA of the optical system as significant as to 0.55 yields an optical resolution 215 nm above that required to resolve the nanostructures. Such a reduction increases the disparity in the vertical axis, however, without a total loss of information in the orientation.

scans of the measured azimuth angle, taken through the pit centers [Fig. 2(a)], are shown in Fig. 2(c) for imaging NAs of 0.55 (black, right axis) and 0.95 (black, left axis). Given our operating wavelength of 405 nm the optical resolution of the 0.95 NA system was calculated to be 240 nm compared to the 200 nm pit separation. Despite such a resolution, good agreement is found between the measured azimuth angle and the expected angular orientation (blue markers) of the pits. The dashed red curve is obtained from simulations using a rigorous model of high-NA imaging systems [14]. Simulations assume an ideal optical system, such that aberrations present in our system account for the small discrepancies with the experimental results. The experimentally observed angular range is 36.21° (instead of 39°), and the greatest deviation from the expected values (blue markers) is 1.17°. Given this error and decrease in angular range, over a full angular range, i.e., 0–180°, (180 × 36.21/39/1.17 =) 143 distinct evenly distributed angles can thus be resolved with our system. In the context of data storage, a single nanostructure can thus encode $\log_2(143) \approx 7$ bits; which represents a sevenfold increase in storage capacity compared to existing binary technologies. This result represents an important step from binary toward $m$-nary storage systems.

With reference to Fig. 2, we note that the measured angular range in this case is 92.85% of the actual range (39°). Reducing the NA of the optical system to 0.55, yielding an optical resolution of 415 nm, increases the difference between expected and measured angular ranges. However, information in the azimuth angle is still present (black solid line), although the magnitude of the angular error also increases. In this case, 22 distinct angles could be resolved. In general, the difference between the experimental and theoretical angular ranges arises due to unavoidable cross talk occurring in the irradiance domain, from which the azimuthal angle is derived, as can be seen from Eq. (1). Geometrically, Eq. (1) states that the observed Stokes vector $\mathbf{S}(x)$ is dictated by the vector sum, weighted by the PSF, of the individual Stokes vectors $(\mathbf{S}_1, \ldots, \mathbf{S}_i, \ldots, \mathbf{S}_n)$ originating from each dipole source, as depicted schematically in Fig. 3(a) (with $i = 4$). The resultant vector $\mathbf{S}(x)$ will, in general, have an azimuth angle most similar to that of the vector with greatest magnitude. Physically this corresponds to the orientation of the dipole source lying closest to the center of the PSF [e.g., $x = x_4$ in Fig. 3(a)]. Accordingly, reducing the system NA increases the area of illumination in the sample, resulting in more uniform illumination of multiple nanostructures and, hence, larger cross talk. Consequently, a reduced angular variation is observed.

Interestingly, reducing the NA has a greater detrimental effect on the resolution of irradiance measurements than on the corresponding measurements of the azimuth angle. This is illustrated in Figs. 3(b) and 3(c), which show a series of line scans for measurements with different system NAs, when illuminating with unpolarized light. The plots are normalized by their mean for comparison purposes. As expected, the information in the irradiance is rapidly lost as the NA reduces, while the information in the azimuth angle is more robust.

Moreover, complete Stokes vector polarimetry [15] allows inference of numerous physical quantities describing an electric field, such as the DOP, azimuth angle of the polarization, retardant, and irradiance, whereas

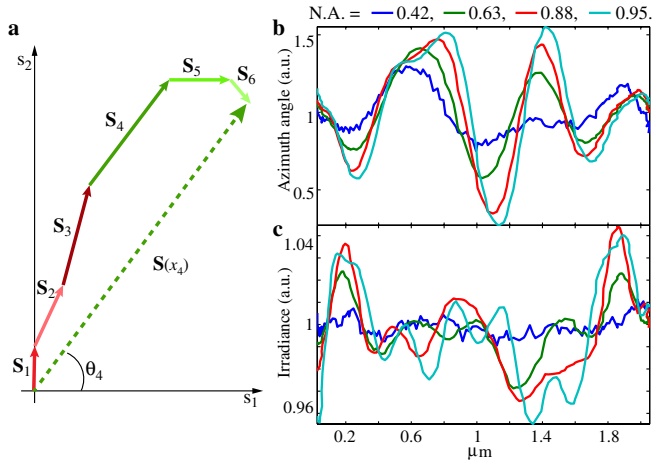


Fig. 3. Effect of imaging with different NA on the azimuth angle of the polarization and irradiance. (a) shows an example of the geometrical vector sum of six Stokes vectors with a weight (given by a PSF) and resultant $\mathbf{S}(x)$, as proposed by Eq. (1). Changing the NA modifies the weighting factor of the Stokes vectors and hence affects the azimuth angle of the $\mathbf{S}(x)$. (b) and (c) show line scans of the measured azimuth angle and irradiance of a track in the set of nanostructures with different NAs. Decreasing the NA affects drastically the irradiance compared to the azimuth angle.

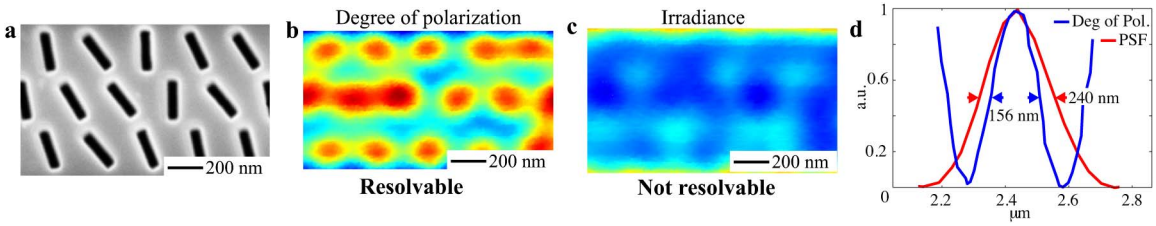


Fig. 4. Resolution in polarization imaging. (a) SEM image of the nanostructures. (b) Spatial distribution of the DOP and (c) irradiance obtained when imaging the nanostructures with unpolarized light. (d) Comparison of the experimental PSF of the optical system (red) and a cross section from a feature in (b) (blue); the respective full width at half-maxima are displayed in the figure. It is possible to resolve the position of the nanostructures using the spatial distribution of the DOP, while the irradiance remains resolution limited.

complete Mueller matrix polarimetry [15] yields physical characterization of a sample in terms of quantities such as diattenuation, polarizance, depolarization, and retardation [15]. Interestingly, some of these quantities display intriguing imaging properties. For example, when imaging the nanostructures [Fig. 4(a)] with unpolarized light, it is possible to resolve their position from the spatial distribution of the DOP [Fig 4(b)], while the irradiance cannot [Fig 4(c)]. Comparing the PSF of the system, which was previously measured using a 100 nm gold bead, and the cross section of a feature in the DOP [Fig 4(b)] reveals an increase in the polarization resolution of the system. The improvement in general is by a factor of 2 and is due to the definition of the DOP, i.e., $P = \sqrt{s_1^2 + s_2^2 + s_3^2}/s_0$. In the case of imaging a sinusoidal polarization grating with spatial frequency $\mu$, for example, the spatial distribution of the DOP is modulated by $\sin(2\mu)$. The same increase in polarization resolution is seen in diattenuation, polarizance, and depolarization due to the similarity of their definitions.

In summary, we have demonstrated theoretically and experimentally that polarization imaging does not necessarily follow the same rules as conventional (confocal) irradiance imaging. The important factors in achieving high polarization resolution are the degree of correlation in the focal plane and the area of the confocal detector [7]. Because the fixed dipoles emit fully polarized light, their fields may combine coherently even if they are illuminated with (spatially correlated) unpolarized light, leading to the loss of superresolution. The extent to which the combination occurs depends directly on the degree of correlation present between the fields emitted by the dipoles. We have also shown experimentally that it is possible to resolve the position and orientation of nanostructures below the diffraction limit using the azimuth angle of the polarization and the spatial distribution of the DOP. We have shown that the measured azimuth angle of the polarization can be derived from the simple geometrical vector addition of weighted Stokes vectors, and how decreasing the NA does not result in a total loss of information in the azimuth angle, while it does in the irradiance.

The authors acknowledge help from Prof. Herbert Gross, Dr. Andrew Pauza, and Dr. Attila Tóth, and financial support from the EU FP6 and FP7 programs (Surpass and SLAM), CONACyT, EPSRC, and the Alexander von Humboldt Foundation. P. M. is supported by a Discovery Early Career Research Award from the Australian Research Council ( DE120101331).

## References

1. R. M. A. Azzam and N. M. Bashara, *Ellipsometry and Polarized Light*, 1st ed. (Elsevier, 1987), p. 539.
2. A. De Martino, S. Ben Hatit, and M. Foldyna, Proc. SPIE **6518**, 65180X (2007).
3. O. G. Rodríguez-Herrera, D. Lara, K. Y. Bliokh, E. A. Ostrovskaya, and C. Dainty, Phys. Rev. Lett. **104**, 253601 (2010).
4. K. Lindfors, T. Setälä, M. Kaivola, A. T. Friberg, and T. Seta, J. Opt. Soc. Am. A **22**, 561 (2005).
5. M. Born and E. Wolf, *Principles of Optics*, 2nd ed. (Cambridge University, 1999), p. 952.
6. P. Török, P. Higdon, and T. Wilson, Opt. Commun. **148**, 300 (1998).
7. C. Macias-Romero, M. R. Foreman, and P. Török, Opt. Express **19**, 25066 (2011).
8. J. M. Bueno and M. C. W. Campbell, Opt. Lett. **27**, 830 (2002).
9. D. Lara and C. Dainty, Opt. Lett. **30**, 2879 (2005).
10. J. S. Tyo, D. L. Goldstein, D. B. Chenault, and J. A. Shaw, Appl. Opt. **45**, 5453 (2006).
11. C. Macías-Romero, R. Lim, M. R. Foreman, and P. Török, Opt. Lett. **36**, 1638 (2011).
12. W. Urbaczyk, Opt. Acta **33**, 53 (1986).
13. J. Goodman, *Introduction to Fourier Optics* (Roberts and Company, 2004).
14. P. Török, P. Munro, and E. Kriezis, Opt. Express **16**, 507 (2008).
15. D. Goldstein, *Polarized Light*, 3rd ed. (Taylor & Francis, 2011), p. 770.